OPAL Physics Note PN383
March 12, 1999

# Measurement of the production rate of $b\bar{b}$ quark pairs from gluons and $b\bar{b}b\bar{b}$ events in hadronic $Z^0$ decays

The OPAL Collaboration

**Abstract**

The rate of gluons splitting to $b\bar{b}$ quark pairs per hadronic $Z^0$ decay, $g_{b\bar{b}}$, and the rate of final states with two $b\bar{b}$ quark pairs, $g_{4b}$, are measured, using data collected by OPAL. Events containing four jets are selected where two of the jets that are close in phase-space contain secondary decay vertices. In addition four-jet events are selected that have secondary decay vertices in at least three of the four jets. Information from the event topology is combined in a likelihood analysis to extract the values of $g_{b\bar{b}}$ and $g_{4b}$:

$$\begin{aligned} g_{b\bar{b}} &= (2.15 \pm 0.43(\text{stat}) \pm 0.80(\text{syst})) \times 10^{-3}, \\ g_{4b} &= (0.53 \pm 0.20(\text{stat}) \pm 0.23(\text{syst})) \times 10^{-3}. \end{aligned}$$

# 1 Introduction

Bottom quark pairs in $Z^0$ decays can be produced either directly via $Z^0 \to b\overline{b}$ or indirectly, when a gluon is radiated from a quark and then splits into a $b\overline{b}$ quark pair. The rate for the latter process, $g \to b\overline{b}$, per hadronic $Z^0$ decay, is called $g_{b\overline{b}}$ in this paper. A special case consists of events with both direct and indirect b quark production, $Z^0 \to b\overline{b}g \to b\overline{b}b\overline{b}$. The rate of $b\overline{b}b\overline{b}$ events per hadronic $Z^0$ decay is called $g_{4b}$ here. A simple estimate for $g_{4b}$ is just the rate for direct $b\overline{b}$ production times the rate of indirect $b\overline{b}$ production. This simple picture has to be modified because the phase-space for two $b\overline{b}$ quark pairs is smaller than that for two light and two b quarks.

Interference terms of the secondary $b\overline{b}$ production with primary $b\overline{b}$ production are zero at leading order in $\alpha_s$, except for the $b\overline{b}b\overline{b}$ final state [1, 2]. In [1], the contribution of the interference term for the state $b\overline{b}b\overline{b}$ is shown to be less than 0.2% of $g_{b\overline{b}}$. The rate $g_{b\overline{b}}$ has been calculated in [1], including the re-summation of leading logarithmic terms. The authors point out that the parton-shower approach as implemented in JETSET [3] is a good approximation. Numerical calculations of $g_{b\overline{b}}$ are given in [1, 4], predicting a rate in the range $g_{b\overline{b}}^{\mathrm{theor}} = (1.8 - 2.9) \times 10^{-3}$, depending on the b quark mass and the strong coupling constant. Measurements of $g_{b\overline{b}}$ using four-jet final states have been reported by the ALEPH and DELPHI collaborations, with the results $g_{b\overline{b}} = (2.77 \pm 0.42(\mathrm{stat}) \pm 0.57(\mathrm{syst})) \times 10^{-3}$ [6] and $g_{b\overline{b}} = (2.1 \pm 1.1(\mathrm{stat}) \pm 0.9(\mathrm{syst})) \times 10^{-3}$ [5], in agreement with the theoretical predictions.

The rate of $g \to b\overline{b}$ is an important input to the precise measurements of $R_b$, the rate of $Z^0$ decays to $b\overline{b}$ quark pairs relative to all hadronic decays, where the gluon splitting to $b\overline{b}$ quark pairs is considered as background. Because of the sensitivity of $g_{b\overline{b}}$ and $g_{4b}$ to both the b quark mass and the strong coupling constant $\alpha_s$, measurements of these rates also test Quantum Chromodynamics (QCD).

In this analysis, decays of the $Z^0$ into four-jet final states are investigated. Jets from b or $\overline{b}$ quarks are identified by reconstructing secondary decay vertices. A $b\overline{b}$ quark pair originating from a gluon tends to have a small invariant mass above the threshold of twice the b quark mass, since the probability of radiating a gluon drops rapidly with increasing gluon virtuality (see figure 9b). This leads to a small relative momentum of the two b hadrons produced in the fragmentation process. By contrast, directly produced $b\overline{b}$ quark pairs have high invariant masses, since they carry a large part of the $Z^0$ energy. This and other characteristics are used to select event samples enriched in the process $g \to b\overline{b}$. An angular correlation defined similarly to the Bengtsson-Zerwas angle [7] is used to further differentiate between $q\overline{q}q\overline{q}$ and $q\overline{q}gg$ final states. In addition, events with three reconstructed secondary vertices are selected. They are used to measure the $g_{4b}$ rate.

For this analysis, Monte Carlo simulations are used to evaluate signal and background efficiencies. Simulated events of the gluon splitting to $b\overline{b}$ signal are referred to as $\mathbf{q\overline{q}b\overline{b}}$ ($\mathbf{q = udsc}$), except for the case of gluon splitting in events with a primary $b\overline{b}$ quark pair. These are referred to as $\mathbf{b\overline{b}b\overline{b}}$. The most important sources of background are events with gluon splitting to $c\overline{c}$ and four-jet events with a primary $b\overline{b}$ quark pair. They are referred to as $\mathbf{Q\overline{Q}c\overline{c}}$ ($\mathbf{Q = udscb}$) and $\mathbf{b\overline{b}xx}$ ($\mathbf{x = guds}$), respectively.

# 2 Event selection and reconstruction

## 2.1 The OPAL detector

The OPAL detector is described in detail elsewhere [8]. Only a brief description of the detector elements relevant to this analysis is given here. Charged tracks are reconstructed in the central tracking system. It consists of a silicon microvertex detector, a vertex drift

chamber equipped with axial and stereo wires, a large jet chamber and $z$ chambers[1]. A solenoid providing a uniform magnetic field of 0.435 T parallel to the $z$-axis surrounds the central tracking system. The silicon microvertex detector [9] has two layers which measure tracks in $r\phi$, the inner layer covering the range $|\cos(\theta)| < 0.83$ and the outer layer covering the range $|\cos(\theta)| < 0.77$. This detector has been upgraded twice. After 1993 it has provided a measurement of the $z$ coordinate [10], but the information from the $z$ coordinate measurement in the silicon microvertex detector is not used in this analysis. After 1995 the microvertex has covered the range up to $|\cos\theta| < 0.93$ [11]. The vertex chamber extends over the range $|\cos\theta| < 0.95$. The coil is surrounded by scintillators for time-of-flight measurements and a barrel lead-glass electromagnetic calorimeter. Including the endcap electromagnetic calorimeter, the lead-glass blocks cover the range $|\cos\theta| < 0.98$. The magnetic return yoke is instrumented with streamer tubes and serves as a hadron calorimeter. The hadron calorimeter is in turn surrounded by muon chambers.

### 2.2 Event selection and reconstruction

The analysis uses data taken with the OPAL detector in the years 1992–1995 on or near the $Z^0$ resonance. Hadronic $Z^0$ decays are selected with an efficiency of 98.4%, as described in [12]; this selection is based on the track and cluster multiplicities and on the energy flow in the electromagnetic calorimeter. Only events with the tracking system and the electromagnetic calorimeter fully operational are used in this analysis. A total number of 3.35 million hadronic events are selected. In these events charged tracks and electromagnetic clusters satisfying certain quality criteria are used for the analysis. The most important cut for the charged tracks is the requirement of at least 20 hits in the central jet chamber, a distance of closest approach to the nominal interaction point in the $r\phi$ plane $d_0 < 5\,\mathrm{cm}$, a momentum transverse to the $e^+e^-$ direction $p_t > 0.15\,\mathrm{GeV}$, and $\chi^2 < 100$ for both the track fit in the $r\phi$ plane and the track fit in the $rz$ plane. For the barrel calorimeter a cluster must have an energy greater than 0.1 GeV. In the endcap calorimeter at least two lead glass blocks and a raw energy greater than 0.25 GeV are required for each cluster. The energy of clusters pointed to by charged tracks are corrected for double counting by subtracting the energy deposition expected from the momentum of the track. Details of this method are described in [13].

### 2.3 Simulated events

A total number of 14 million events generated with JETSET [3] are used to evaluate the efficiencies for background and signal, respectively. Within this sample, 1.9 million (4.3 million) events were generated in special runs with a primary $c\overline{c}$ ($b\overline{b}$) quark pair to increase the statistical significance of the description of background processes with secondary decay vertices. In addition, 125 000 events have been generated for the signal process $Z^0 \to q\overline{q}g \to q\overline{q}b\overline{b}$. They are used to evaluate the selection efficiency for the signal with a high statistical precision. All these events were passed through a complete simulation of the OPAL detector [14].

The simulated events are weighted to correspond to the measured values of $c\overline{c}$ and $b\overline{b}$ production, $R_c = 0.1724$ and $R_b = 0.21664$, given in [15]. The rate of gluons splitting to $c\overline{c}$ pairs is set to $g_{c\overline{c}} = 2.38 \times 10^{-2}$ as measured by OPAL [16]. The ratio of the number of events with primary produced b quarks and gluon splitting to $c\overline{c}$ quark pairs to the total number of events with gluon splitting to $c\overline{c}$ quark pairs is fixed to the value predicted by

[1] The OPAL coordinate system is defined with positive $z$-axis along the electron beam direction, the $x$ axis pointing to the centre of the LEP accelerator ring and the $y$-axis normal to the $x$–$z$ plane. $\theta$ and $\phi$ are the polar and azimuthal angles respectively.

JETSET. The rate of gluon splitting to $b\bar{b}$ pairs is set to $g_{b\bar{b}} = 2.0 \times 10^{-3}$ and the rate of $b\bar{b}b\bar{b}$ events is set to $g_{4b} = 0.4 \times 10^{-3}$ for comparisons wit the data.

### 2.4 The four-jet selection

The four-momenta of the selected tracks and clusters are combined to form four jets, using the $k_\perp$ (Durham) algorithm [17]. In this algorithm the jet resolution between two particles $i$ and $j$ is defined as

$$y^{ij} = \frac{2\min(E_i^2, E_j^2)(1-\cos(\theta_{ij}))}{(\sum_k E_k)^2},$$

where $E_i$, $E_j$, $E_k$ are the particle energies and $\theta_{ij}$ is the angle between particle $i$ and $j$. The denominator $(\sum_k E_k)^2$ is the square of the energy sum of all particles used for the jet finding. The two particles with the smallest jet resolution $y^{ij}$ are subsequently combined to form a new pseudo-particle (jet) by adding their four-momenta, and this process is repeated until only four jets are left. For a given configuration of four jets, the variable $y_{34}$ is defined as the minimal $y^{ij}$ of all possible jet pairs. Figure 1 shows normalised distributions of the predicted $g \to b\bar{b}$ signal and all simulated events together with the data as a function of the jet resolution $y_{34}$. The $g \to b\bar{b}$ signal populates the region of high $y_{34}$. A cut $y_{34} > 0.006$ is made to define the four-jet sample. This cut rejects nearly 90% of the background events, but keeps about 60% of the signal events, with an estimated purity of 1%. After applying this cut, a total of 439 525 events is selected in the data. In the Monte Carlo simulation only 382 855 events are selected, when normalising to the total number of hadronic $Z^0$ decays, which corresponds to a deficit of 13%. This deficit might be due to missing higher orders in the parton shower. To deal with this normalisation problem, the number of simulated events is normalised to the number of four-jet events throughout this analysis, instead of normalising to the number of hadronic $Z^0$ decays. The stability of this analysis with respect to variations of the cut in $y_{34}$ is discussed in section 4.4.

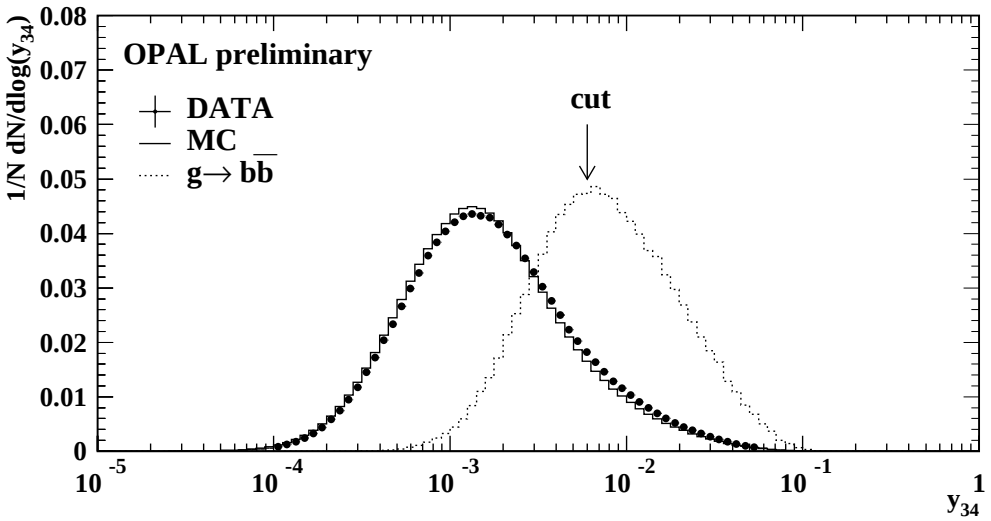


Figure 1: *Normalised distributions of the jet resolution parameter $y_{34}$. The data is shown with dots, the shape predicted from Monte Carlo simulations with a solid line and the shape predicted for the signal events as a dotted line.*

### 2.5 Vertex reconstruction

A primary vertex is reconstructed for each event as described in [18]; the selected tracks are fitted to a common vertex, using also the beam spot position. In an iterative procedure, tracks with a large contribution to the $\chi^2$ are removed, and the fit is repeated until every track contributes less than 4 to $\chi^2$.

For each jet, a secondary vertex is reconstructed, using the full three-dimensional tracking information [19]. All tracks in the jet with a momentum $p > 0.5\,\mathrm{GeV}$, a distance $d_0 < 0.3\,\mathrm{cm}$ to the fitted primary vertex in the $r/\phi$ plane and an error on $d_0$ of $\sigma_{d_0} < 0.1\,\mathrm{cm}$ are fitted to a common vertex. These criteria select well measured tracks, the momentum cut preferentially selects tracks from the decay of b hadrons rather than those produced in the fragmentation process. Tracks with a large $\chi^2$ contribution are removed until the overall $\chi^2$ is smaller than 4. If three or more tracks remain, the secondary vertex is accepted.

The decay length $l$ and its error $\sigma$ are calculated as the distance of the primary to the secondary vertex, the direction constrained to be parallel to the jet axis. The sign of $l$ is positive if the angle between the jet axis and the vector pointing from the primary to the secondary vertex is less than 90 degrees, negative otherwise. Vertices with $l > 0$ are used to identify b hadrons. In this analysis, the following variables are used to identify secondary vertices originating from the decay of b hadrons:

- The decay length significance $l/\sigma$.
- The output of a neural network $a^{\mathrm{NN}}$ that has been trained to separate vertices originating from b hadron decay from those in charm or light quark events. The neural network is described in detail in [19]. It is only applied when $l/\sigma > 3$. It has five inputs: the decay length significance $l/\sigma$, the decay length $l$, the number of tracks in the secondary vertex $n_s$, the reduced decay length $l_r/\sigma_r$, where one track has been removed from the vertex fit, and a variable $x_D$, sensitive to the invariant mass of the tracks in the jet that have a high probability of originating from a b hadron decay. The neural network output $a^{\mathrm{NN}}$ lies between zero and one. Values close to one indicate a high probability that the vertex is associated with a b hadron decay.

## 3 Analysis

In subsection 3.1 the selection of candidate events for gluon splitting will be described, where the four jets are sorted by the topology imposed on the event by the $k_\perp$ jet finder to define two gluon splitting candidate jets. The candidate jets are checked for secondary vertices and events with two significant secondary vertices are selected. The event sample is subdivided into two distinct classes, depending on the event topology. Different cuts on the neural network output are applied for each class, to define the candidate events. In subsection 3.2 the selection of candidates for the process $\mathrm{Z}^0 \to \mathrm{b\overline{b}b\overline{b}}$ is discussed, where all four jets are checked for secondary vertices.

Finally, in subsection 3.3 the rate of gluon splitting to $\mathrm{b\overline{b}}$ is calculated. For each of the selected event samples angular distributions sensitive to four quark final states are studied. The rate of gluon splitting and the rate of $\mathrm{b\overline{b}b\overline{b}}$ events are then calculated using a binned maximum likelihood fit with the selection efficiencies and these distributions as input.

### 3.1 The $\mathrm{q\overline{q}b\overline{b}}$ event selection

The four-jet events are clustered to three jets, using the $k_\perp$ scheme. Those two jets that are combined to one jet in this step are considered to be candidates for $\mathrm{g} \to \mathrm{b\overline{b}}$. This is motivated by the small relative momentum expected for two jets from the process $\mathrm{g} \to \mathrm{b\overline{b}}$,

which results in a small value for the jet resolution $y^{ij}$ for this jet pair. In a next step, the three-jet event is clustered to two jets. There are two distinct possibilities for this, as shown in figure 2:

**Class "2+2":** Events belong to this class if the two jets, which are clustered when going from three to two jets, are the two jets that have not been clustered when going from four to three jets.

**Class "3+1":** Events belong to this class if one of the jets that is clustered when going from three to two jets is the jet that was formed from the two $g \to b\overline{b}$ candidates when going from four to three jets.

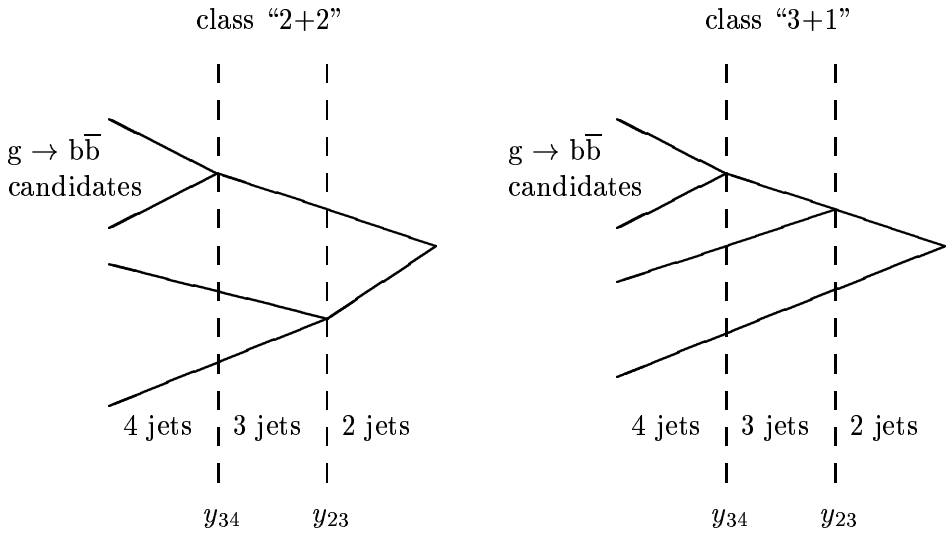


Figure 2: *Illustration of the definition of class "2+2" and class "3+1" and the* $g \to b\overline{b}$ *candidate jet selection.*

This procedure selects 232 860 events in class "2+2" and 206 665 events in class "3+1". The Monte Carlo simulation predicts 239 060 and 200 465 events, respectively. Implications on the final result for $g_{b\overline{b}}$ and $g_{4b}$ from this statistically significant difference in the number of observed to expected events in those two event classes are considered in the discussion of the experimental uncertainties.

The two candidate jets are now checked for secondary vertices. If both jets have secondary vertices with $l/\sigma > 3$, the event is selected. This cut is studied in figure 3. It shows the decay length significance of the jet with the smaller decay length significance. If this variable $(l/\sigma)_2$ is larger than 3, the event is selected, otherwise it is rejected. Because only the smaller decay length significance of the two vertices enters this distribution, there are more entries at negative values of $(l/\sigma)_2$. The cut $(l/\sigma)_2 > 3$ reduces the background from events with light flavours and it also reduces the fraction of events from the $g \to c\overline{c}$ process.

In the next step the neural network output is calculated for both vertices in the selected events. The two $g \to b\overline{b}$ candidates are ordered by the neural network output $a^{NN}$ assigned to their secondary vertex such that $a_1^{NN} > a_2^{NN}$. Figure 4 shows the variables $a_1^{NN}$ and $a_2^{NN}$, separately for the event classes "2+2" and "3+1".

Note that most events arise from primary $b\overline{b}$ production. The $g \to b\overline{b}$ signal fraction is located at high values of $a_1^{NN}$, for both event classes, but for event class "2+2" the background from primary $b\overline{b}$ quark production shows a similar behaviour to the signal.

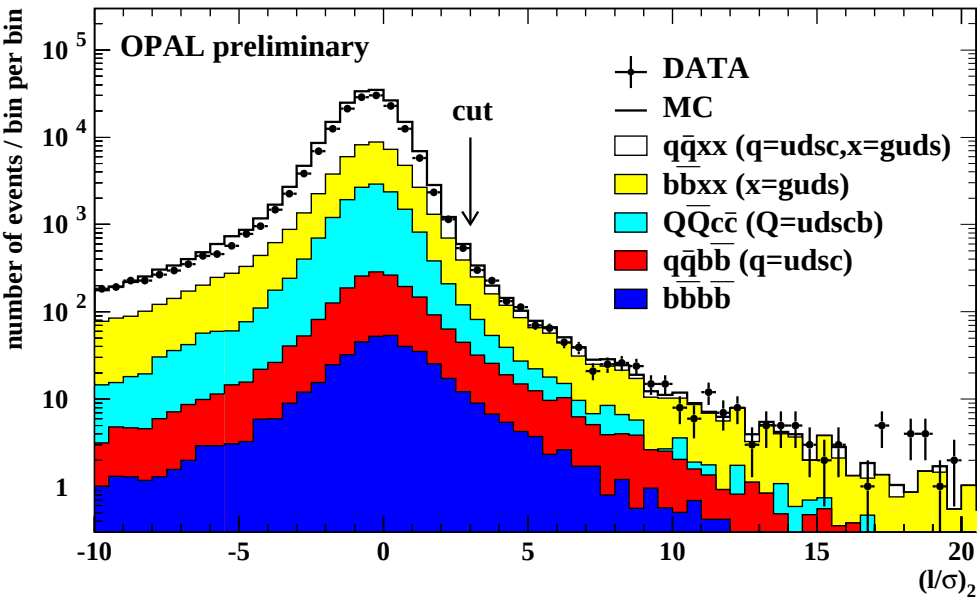


Figure 3: *The decay length significance* $(l/\sigma)_2$ *of the* $g \to b\bar{b}$ *candidate jet with the smallest decay length significance. The cut value is indicated by an arrow. The points show data and the histogram shows the Monte Carlo simulation. The contributions from various four-jet processes are indicated.*

The variable $a_2^{\mathrm{NN}}$ shows a larger fraction of background events at lower values in class "2+2", but less sensitivity in class "3+1". To enrich the signal, cuts in $a_1^{\mathrm{NN}} > 0.7$ for class "3+1" and $a_2^{\mathrm{NN}} > 0.7$ for class "2+2" are chosen. After applying these cuts, essentially all the background consists of four-jet events with true b hadrons, $b\bar{b}xx$ (x = guds), and a smaller number of events with gluon splitting to $c\bar{c}$, $Q\bar{Q}c\bar{c}$ (Q = udscb).

Finally the other two jets that were not considered to be gluon splitting candidates, are checked for secondary vertices. These jets are denoted as "primary jet candidates". If both of these jets have a vertex, only the jet with the larger decay length significance is considered. Figure 5 shows the distribution of the decay length significance of this vertex, $(l/\sigma)_{\mathrm{prim}}$. The variable $(l/\sigma)_{\mathrm{prim}}$ shows some separation between the $b\bar{b}b\bar{b}$ events and the other events contributing to the $g \to b\bar{b}$ signal. A cut $(l/\sigma)_{\mathrm{prim}} > 2$ is made to define event samples enriched or depleted with $b\bar{b}b\bar{b}$ events. The following four event samples are defined

**sample A:** events that satisfy all cuts in class "2+2" and the condition $(l/\sigma)_{\mathrm{prim}} > 2$.

**sample B:** events that satisfy all cuts in class "2+2" but fail the condition $(l/\sigma)_{\mathrm{prim}} > 2$ or have no secondary vertex at all in the primary jet candidates.

**sample C:** events that satisfy all cuts in class "3+1" and the condition $(l/\sigma)_{\mathrm{prim}} > 2$.

**sample D:** events that satisfy all cuts in class "3+1" but fail the condition $(l/\sigma)_{\mathrm{prim}} > 2$ or have no secondary vertex at all in the primary jet candidates.

### 3.2 The $b\bar{b}b\bar{b}$ event selection

To select $b\bar{b}b\bar{b}$ final states, events where at least three of the four b hadrons are reconstructed are selected. The variables used are shown in figure 6. Significant secondary vertices are

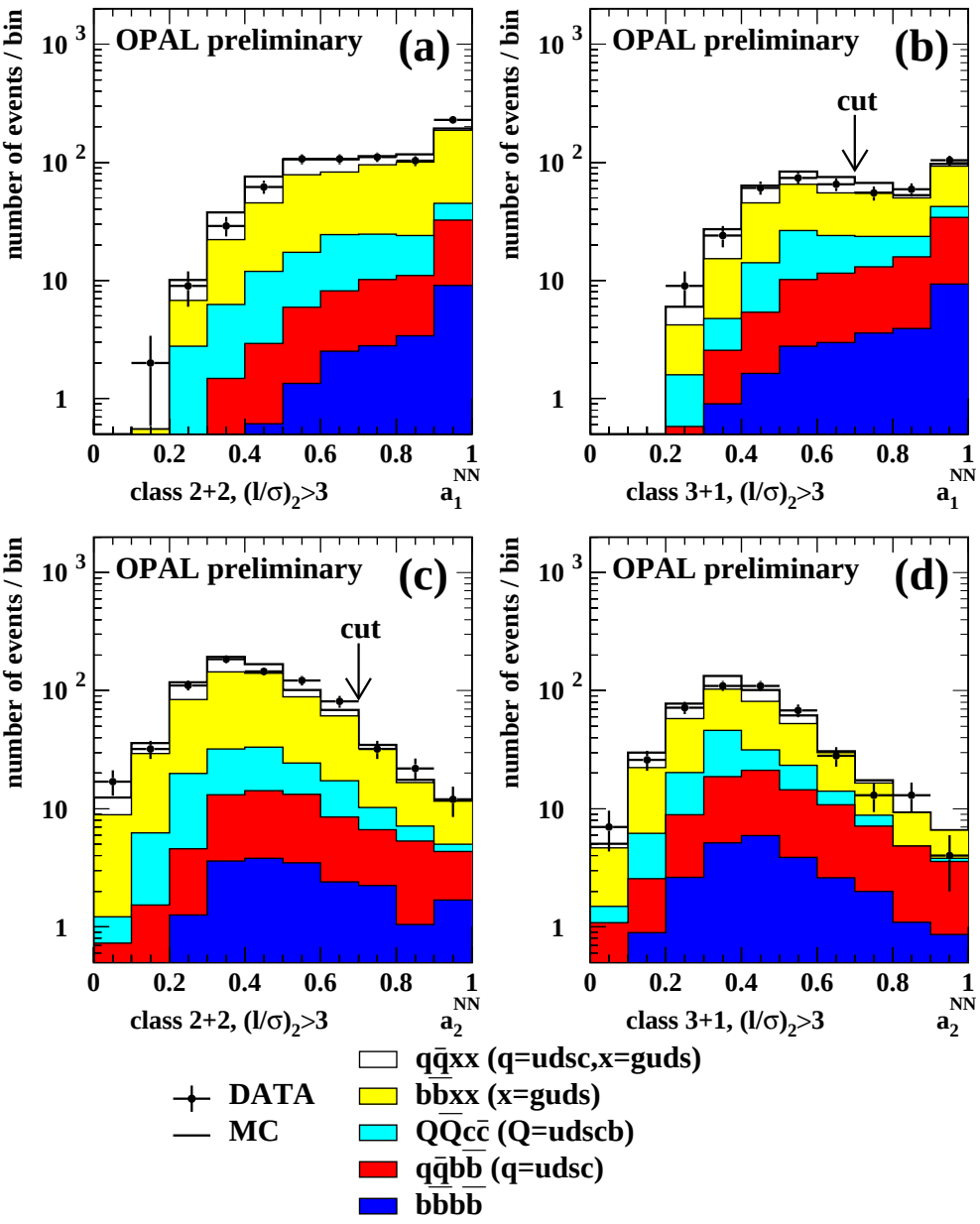


Figure 4: *The neural network outputs* $a_1^{\rm NN}$ *and* $a_2^{\rm NN}$ *of the two* $\rm g \to b\overline{b}$ *candidate jets in the event classes "2+2"and "3+1", for events with two significant secondary vertices. (a) class "2+2"* $a_1^{\rm NN}$*, (b) class "3+1",* $a_1^{\rm NN}$*, (c) class "2+2"* $a_2^{\rm NN}$*, (d) class "3+1"* $a_2^{\rm NN}$*. The points show data and the histogram shows the Monte Carlo simulation. The contributions from various four-jet processes are indicated. The arrows in (b) and (c) indicate the position of the cuts.*

reconstructed in at least three of the four jets, with $l/\sigma > 3$. Figure 6a illustrates the selection of three significant vertices, showing the third largest decay length significance, denoted $(l/\sigma)_3$. The $\rm b\overline{b}b\overline{b}$ signal is enhanced for large values of this variable. The cut $(l/\sigma)_3 > 3$ suppresses light flavours, most of the $\rm g \to c\overline{c}$ events, and also the $\rm g \to b\overline{b}$ events with a light primary quark. Figure 6b shows the third largest neural network output $a_3^{\rm NN}$ for all selected vertices. The background mainly dominates the region of low $a_3^{\rm NN}$, while the $\rm b\overline{b}b\overline{b}$ signal extends to high values of $a_3^{\rm NN}$. About half of the events shown in this plot are

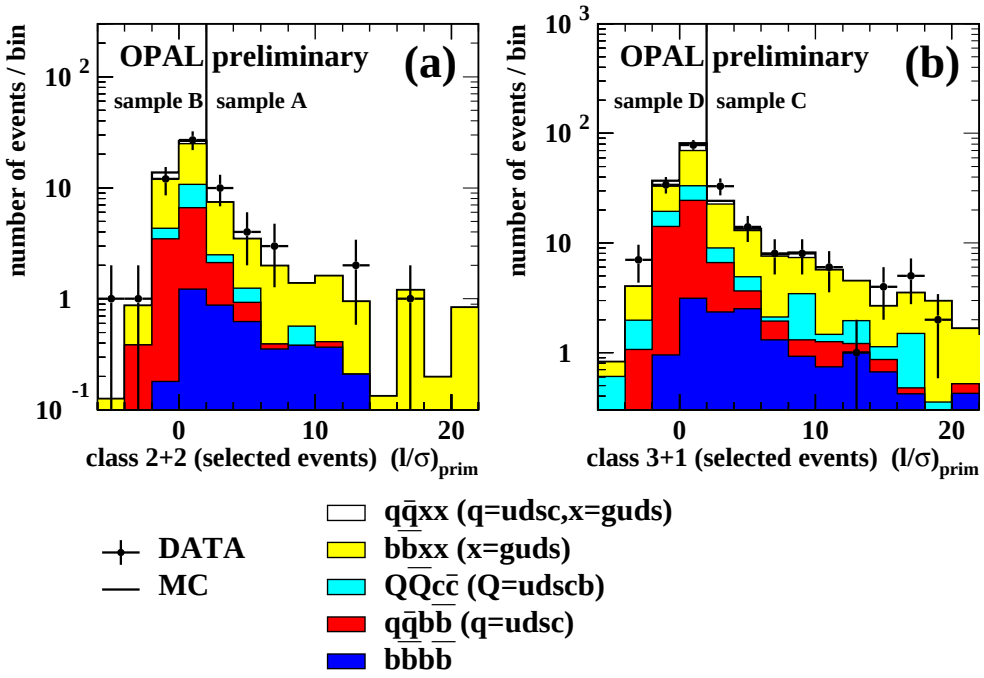


Figure 5: *Largest decay length significance $l/\sigma_{\rm prim}$ of the primary jet candidates, as defined in the text, after applying all selection cuts for the* $\rm q\bar{q}b\bar{b}$ *selection. Events from class "2+2" appear in figure 5a, events from class "3+1" in figure 5b. The points show data and the histogram shows the Monte Carlo simulation. The contributions from various four-jet processes are indicated. The vertical lines at $(l/\sigma)_{\rm prim} = 2$ indicate the cut to separate the event samples A from B and C from D.*

already selected in the event samples A or C. To avoid double counting, these events have been removed from the $\rm b\bar{b}b\bar{b}$ selection. The resulting distribution of $a_3^{\rm NN}$ is shown in 6c, with a similar behaviour for the background and signal shapes as observed in figure 6b. A cut $a_3^{\rm NN} > 0.7$ is chosen to select the final $\rm b\bar{b}b\bar{b}$ candidates here, denoted as sample E.

### 3.3 Calculation of $g_{\rm b\bar{b}}$ and $g_{\rm 4b}$

After applying all cuts, 310 events remain in the samples A–E, where the simulation with $g_{\rm b\bar{b}} = 2.0 \times 10^{-3}$ and $g_{\rm 4b} = 0.4 \times 10^{-3}$ predicts 306 events. The efficiencies for selecting signal events, $\rm g \to b\bar{b}$ with a light primary flavour or $\rm b\bar{b}b\bar{b}$ events, are denoted $\epsilon_{\rm q\bar{q}b\bar{b}}$ and $\epsilon_{\rm b\bar{b}b\bar{b}}$. The total efficiencies as obtained from JETSET are $\epsilon_{\rm q\bar{q}b\bar{b}} = 0.92\%$ and $\epsilon_{\rm b\bar{b}b\bar{b}} = 1.88\%$. Table 1 summarises the number of selected events for the cuts applied, and the efficiencies to select signal or background reactions.

In order to extract $g_{\rm b\bar{b}}$, the angle $\alpha_{1234}$ between the plane formed by the two jets that are clustered to one jet when going from a four-jet configuration to a three jet configuration, and the plane containing the two other jets is studied separately for the event classes A–E in figure 7. The definition of this angle $\alpha_{1234}$ is similar to the angular correlation proposed in [7] to measure the QCD colour factors. It can be used to distinguish events with two quarks and two gluons from events with four quarks. In all five event samples the agreement between the data and the Monte Carlo prediction is good. The signal is preferential at high values of $\alpha_{1234}$ while the background has a flat distribution,

The differences in the shape are, however, not large enough to allow the extraction of the signal fractions with high statistical precision. Therefore a maximum likelihood fit

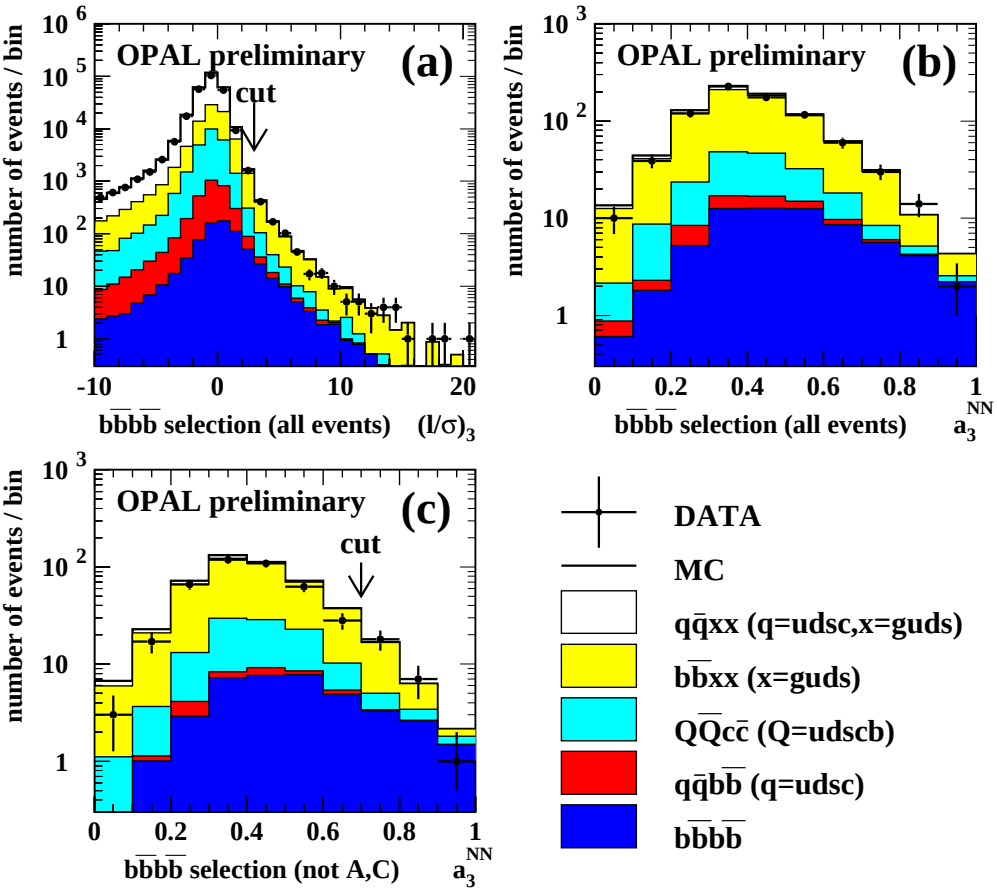


Figure 6: *Plot (a) shows the third largest decay length significance $(l/\sigma)_3$ from the four jets, plot (b) the third largest neural network output $a_3^{\mathrm{NN}}$ for events selected with $(l/\sigma)_3 > 3$, plot (c) the variable $a_3^{\mathrm{NN}}$ as in (b) but with the events removed that are already selected in samples A or C. The points show data and the histogram shows the Monte Carlo simulation. The contributions from various four-jet processes are indicated. Arrows indicate the position of the cuts: in (a) the cut to select three significant vertices, in (c) the cut to select the event sample E.*

of the 25 bins in $\alpha_{1234}$ shown in figure 7 is performed to extract $g_{\mathrm{b\bar{b}}}$ and $g_{4\mathrm{b}}$, assuming Poisson distributions calculated from the signal and background efficiencies for each bin. The likelihood function is given by

$$-\ln\mathcal{L} = \sum_{i=1}^{25}(m_i - d_i \ln m_i) + \mathrm{const},$$

where $d_i$ is the number of observed events in bin $i$ and $m_i$ is the corresponding number of expected events. The latter is given by

$$m_i = N_{4-\mathrm{jet}} \frac{(1-g_{\mathrm{c\bar{c}}}-g_{\mathrm{b\bar{b}}})\epsilon^i_{\mathrm{q\bar{q}}} + g_{\mathrm{c\bar{c}}}\epsilon^i_{\mathrm{q\bar{q}c\bar{c}}} + (g_{\mathrm{b\bar{b}}}-g_{4\mathrm{b}})\epsilon^i_{\mathrm{q\bar{q}b\bar{b}}} + g_{4\mathrm{b}}\epsilon^i_{\mathrm{b\bar{b}b\bar{b}}}}{(1-g_{\mathrm{c\bar{c}}}-g_{\mathrm{b\bar{b}}})\epsilon^{4-\mathrm{jet}}_{\mathrm{q\bar{q}}} + g_{\mathrm{c\bar{c}}}\epsilon^{4-\mathrm{jet}}_{\mathrm{q\bar{q}c\bar{c}}} + (g_{\mathrm{b\bar{b}}}-g_{4\mathrm{b}})\epsilon^{4-\mathrm{jet}}_{\mathrm{q\bar{q}b\bar{b}}} + g_{4\mathrm{b}}\epsilon^{4-\mathrm{jet}}_{\mathrm{b\bar{b}b\bar{b}}}},$$

where $N_{4-\mathrm{jet}}$ is the total number of selected four-jet events used for this analysis. The relative rate of gluons splitting to $\mathrm{c\bar{c}}$ per hadronic $\mathrm{Z}^0$ decay is denoted $g_{\mathrm{c\bar{c}}}$. The rates for the $\mathrm{g} \to \mathrm{b\bar{b}}$ process (including $\mathrm{b\bar{b}b\bar{b}}$ events) and the $\mathrm{b\bar{b}b\bar{b}}$ process are called $g_{\mathrm{b\bar{b}}}$ and $g_{4\mathrm{b}}$,

| | Number of events | | Signal eff. | | Background eff. | |
|---|---|---|---|---|---|---|
| | DATA | MC | $\epsilon_{q\bar{q}b\bar{b}}$ | $\epsilon_{b\bar{b}b\bar{b}}$ | $\epsilon_{q\bar{q}c\bar{c}}$ | $\epsilon_{q\bar{q}}$ |
| The four-jet selection | | | | | | |
| Total four-jet | 439 525 | 439 525 | 57.59% | 60.31% | 34.60% | 10.58% |
| "2+2" | 232 860 | 239 060 | 26.02% | 25.44% | 17.60% | 5.79% |
| "3+1" | 206 665 | 200 465 | 31.56% | 34.86% | 17.00% | 4.78% |
| Event selection in Class "2+2" | | | | | | |
| $(l/\sigma)_2 > 3$ | 760 | 761 | 0.83% | 1.29% | 0.091% | 0.0159% |
| $a_2^{\mathrm{NN}} > 0.7$ | 66 | 64 | 0.18% | 0.32% | 0.007% | 0.0011% |
| Sample A | 22 | 22 | 0.03% | 0.22% | 0.001% | 0.0004% |
| Sample B | 44 | 42 | 0.15% | 0.10% | 0.005% | 0.0007% |
| Event selection in Class "3+1" | | | | | | |
| $(l/\sigma)_2 > 3$ | 451 | 473 | 1.09% | 1.63% | 0.072% | 0.0082% |
| $a_1^{\mathrm{NN}} > 0.7$ | 218 | 217 | 0.74% | 1.08% | 0.028% | 0.0033% |
| Sample C | 90 | 87 | 0.12% | 0.79% | 0.010% | 0.0015% |
| Sample D | 128 | 130 | 0.62% | 0.29% | 0.018% | 0.0018% |
| The dedicated $b\bar{b}b\bar{b}$ selection | | | | | | |
| $(l/\sigma)_3 > 3$ | 792 | 832 | 0.26% | 4.24% | 0.122% | 0.0167% |
| remove overlap | 431 | 481 | 0.09% | 2.51% | 0.081% | 0.0095% |
| $a_3^{\mathrm{NN}} > 0.7$ | 26 | 25 | 0.002% | 0.48% | 0.003% | 0.0004% |
| Sample E | 26 | 25 | 0.002% | 0.48% | 0.003% | 0.0004% |
| **Selected (A–E)** | 310 | 306 | 0.92% | 1.88% | 0.038% | 0.0048% |

Table 1: *The number of events selected at the different steps of the analysis (column DATA) and number of events expected from the simulation with a* $g \to b\bar{b}$ *signal of* $g_{b\bar{b}} = 0.4 \times 10^{-3}$ *and a* $b\bar{b}b\bar{b}$ *signal* $g_{4b} = 0.4 \times 10^{-3}$ *(column MC). Also shown are the efficiencies to select signal or background events, as predicted from the Monte Carlo simulation. The efficiencies to select the signal events with a light primary quark are denoted* $\epsilon_{q\bar{q}b\bar{b}}$*, and the* $b\bar{b}b\bar{b}$ *signal events are denoted* $\epsilon_{b\bar{b}b\bar{b}}$*. The efficiency to select background from gluon splitting to* $c\bar{c}$ *is called* $\epsilon_{q\bar{q}c\bar{c}}$*, for other background sources* $\epsilon_{q\bar{q}}$*.*

respectively. These two variables are taken as the free parameters in the fit. The efficiencies to select the signal process for primary light quarks and the $b\bar{b}b\bar{b}$ events in bin $i$ are denoted $\epsilon^i_{q\bar{q}b\bar{b}}$ and $\epsilon^i_{b\bar{b}b\bar{b}}$, while $\epsilon^i_{q\bar{q}c\bar{c}}$ and $\epsilon^i_{q\bar{q}}$ are the efficiencies to select the $g \to c\bar{c}$ events or other background events in bin $i$. Finally $\epsilon^{4-\mathrm{jet}}_{q\bar{q}b\bar{b}}$, $\epsilon^{4-\mathrm{jet}}_{b\bar{b}b\bar{b}}$, $\epsilon^{4-\mathrm{jet}}_{q\bar{q}c\bar{c}}$, $\epsilon^{4-\mathrm{jet}}_{q\bar{q}}$ are the efficiencies for events in the signal and the background channels to pass the four-jet selection. The likelihood analysis leads to the result

$$g_{b\bar{b}} = (2.15 \pm 0.43(\mathrm{stat.})) \times 10^{-3},$$

$$g_{4b} = (0.53 \pm 0.20(\mathrm{stat.})) \times 10^{-3},$$

where the error is from the finite data statistics only. The correlation coefficient between $g_{b\bar{b}}$ and $g_{4b}$ is 0.066. As an additional cross-check a simple likelihood fit of the normalised signal and background shapes has been done, calculating directly the fractions of $q\bar{q}b\bar{b}$ and $b\bar{b}b\bar{b}$ events in the final event selection. Using the number of selected events, the total number of hadronic $Z^0$ decays and the signal efficiencies, $g_{b\bar{b}}$ and $g_{4b}$ can be calculated from these event fractions. This procedure avoids the necessity to know the absolute selection efficiency for the background. To gain enough sensitivity for this shape fit, each of the 25 bins in the

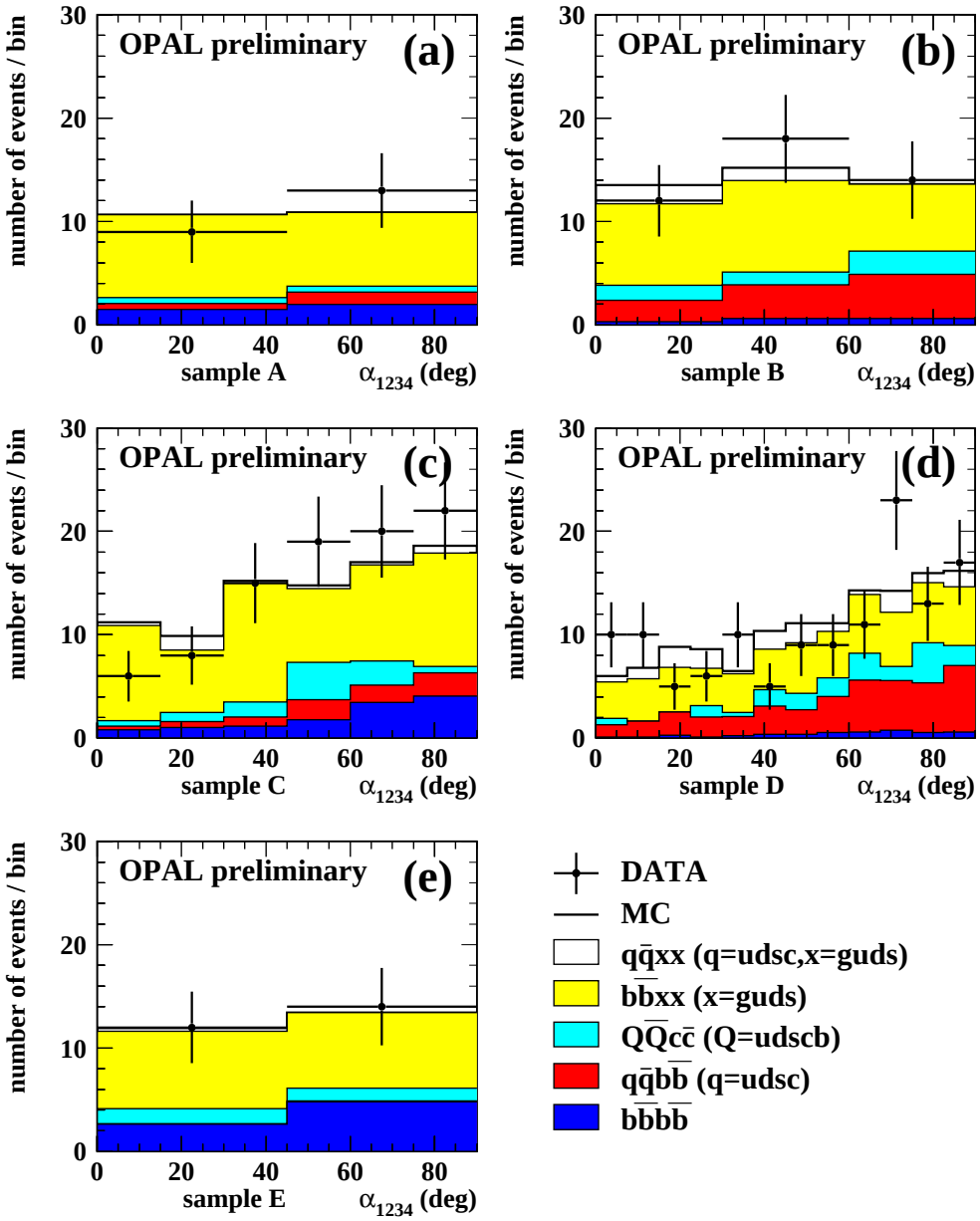


Figure 7: *The angle $\alpha_{1234}$ between the plane formed by the two $g \to b\bar{b}$ candidate jets and the plane formed by the other two jets for the $g \to b\bar{b}$ candidate events after applying all cuts. The figures a–e correspond to the event samples A–E. Data is shown as full points with error bars, the Monte Carlo simulation as a solid line. The contribution from primary $b\bar{b}$ production is shown in light gray, the contribution from gluon splitting to $c\bar{c}$ in grey. The $g \to b\bar{b}$ signal is drawn in dark grey with the contribution from $b\bar{b}b\bar{b}$ events in darker grey.*

final selection is split into two sub-bins of low $y_{34}$ ($y_{34} < 0.014$) and high $y_{34}$ ($y_{34} > 0.014$). The shape fit using these 50 bins leads to the results $g_{b\bar{b}}^{\text{shape}} = (2.90 \pm 0.77) \times 10^{-3}$ and $g_{4b}^{\text{shape}} = (0.62 \pm 0.26) \times 10^{-3}$, with a statistical correlation 0.48. This result, which extracts most of the information from the shapes of the distributions, is considered as a consistency check of the likelihood analysis, which is dominated by the information in the selection

efficiencies for signal and background events. Alternatively, the likelihood fit was repeated using only the individual signal and background selection efficiencies of the event samples A–E given in table 1. The result of this five-bin fit is $g_{\mathrm{b\overline{b}}}^{\mathrm{five}} = (2.02 \pm 0.44) \times 10^{-3}$ and $g_{\mathrm{4b}}^{\mathrm{five}} = (0.47 \pm 0.20) \times 10^{-3}$ with a statistical correlation 0.086. It has been checked that this result is compatible with the central result within the independent statistical errors.

# 4 Cross-checks and evaluation of systematic uncertainties

## 4.1 Flavour composition and tagging efficiencies in the four-jet sample

A cross-check of the flavour composition and the tagging efficiencies of the four-jet selection is important because the four jet sample is used for normalisation and the analysis is quite sensitive to the selection efficiencies for signal and background processes. This cross-check has been done by performing a simultaneous measurement of $R_{\mathrm{b}}$ and the efficiency to tag b jets, using a double tag method.

In each event the two most energetic jets are selected. This ensures that the analysis is mainly sensitive to primary heavy quark production $\mathrm{Z}^0 \to \mathrm{b\overline{b}}$. The jet with the highest energy is denoted jet 1, the other jet 2. Then the tagging variable is checked for both jets, and three statistically independent numbers are extracted:

- $T_1$ the number of events with a tag in jet 1 but not in jet 2.
- $T_2$ the number of events with a tag in jet 2 but not in jet 1.
- $T_{12}$ the number of events with a tag in both jet 1 and jet 2.

Two analyses are possible, one assuming an equal average tagging efficiency for jet 1 and jet 2, the other assuming different tagging efficiencies for jet 1 and jet 2. In the first case, the following set of equations is used

$$\begin{aligned} T_1 + T_2 + 2T_{12} &= 2N_{4-\mathrm{jet}}(R_{\mathrm{b}}\epsilon^{\mathrm{b}} + R_{\mathrm{c}}\epsilon^{\mathrm{c}} + (1 - R_{\mathrm{b}} - R_{\mathrm{c}})\epsilon^{\mathrm{uds}}), \\ T_{12} &= N_{4-\mathrm{jet}}(C^{\mathrm{b}}R_{\mathrm{b}}(\epsilon^{\mathrm{b}})^2 + R_{\mathrm{c}}(\epsilon^{\mathrm{c}})^2 + (1 - R_{\mathrm{b}} - R_{\mathrm{c}})(\epsilon^{\mathrm{uds}})^2), \end{aligned}$$

where $\epsilon^{\mathrm{b}}$, $\epsilon^{\mathrm{c}}$ and $\epsilon^{\mathrm{uds}}$ are the per-jet tagging efficiencies for $\mathrm{b\overline{b}}$, $\mathrm{c\overline{c}}$ and light quark events. $C^{\mathrm{b}} = \epsilon^{2\mathrm{b}}/(\epsilon^{\mathrm{b}})^2$ is the tagging correlation between the two jets for $\mathrm{b\overline{b}}$ events, with $\epsilon^{2\mathrm{b}}$ being the efficiency to tag both jets in a $\mathrm{b\overline{b}}$ event. The tagging correlations for $\mathrm{c\overline{c}}$ or light flavoured events have been neglected. When taking $\epsilon^{\mathrm{c}}$, $\epsilon^{\mathrm{uds}}$ and $C^{\mathrm{b}}$ as inputs from simulated events, $R_{\mathrm{b}}$ and the tagging efficiency $\epsilon^{\mathrm{b}}$ can be extracted from the data. The same analysis can be performed on simulated events to check for biases introduced by neglecting hemisphere correlations for the $\mathrm{c\overline{c}}$ or light flavoured events.

A more detailed analysis assumes different tagging efficiencies for the highest energetic jet and the less energetic jet. The corresponding formulas are

$$\begin{aligned} T_1 + T_{12} &= N_{4-\mathrm{jet}}(R_{\mathrm{b}}\epsilon_1^{\mathrm{b}} + R_{\mathrm{c}}\epsilon_1^{\mathrm{c}} + (1 - R_{\mathrm{b}} - R_{\mathrm{c}})\epsilon_1^{\mathrm{uds}}), \\ T_2 + T_{12} &= N_{4-\mathrm{jet}}(R_{\mathrm{b}}\epsilon_2^{\mathrm{b}} + R_{\mathrm{c}}\epsilon_2^{\mathrm{c}} + (1 - R_{\mathrm{b}} - R_{\mathrm{c}})\epsilon_2^{\mathrm{uds}}), \\ T_{12} &= N_{4-\mathrm{jet}}(C^{\mathrm{b}}R_{\mathrm{b}}\epsilon_1^{\mathrm{b}}\epsilon_2^{\mathrm{b}} + R_{\mathrm{c}}\epsilon_1^{\mathrm{c}}\epsilon_2^{\mathrm{c}} + (1 - R_{\mathrm{b}} - R_{\mathrm{c}})\epsilon_1^{\mathrm{uds}}\epsilon_2^{\mathrm{uds}}), \end{aligned}$$

where the efficiencies are evaluated separately for jet 1 and jet 2. The tagging correlation is given by $C^{\mathrm{b}} = \epsilon^{2\mathrm{b}}/\epsilon_1^{\mathrm{b}}\epsilon_2^{\mathrm{b}}$.

Table 2 summarises the results for two different cuts to define a b tag. The first method

| Assume the same efficiency for both jets | | | |
|---|---|---|---|
| $l/\sigma > 3$ | DATA | MC | MC, true |
| $R_{\mathrm{b}}$ | $0.2138 \pm 0.0031$ | $0.2055 \pm 0.0016$ | 0.2069 |
| $\epsilon^{\mathrm{b}}$ | $0.2603 \pm 0.0030$ | $0.2563 \pm 0.0015$ | 0.2549 |
| $a^{\mathrm{NN}} > 0.7$ | DATA | MC | MC, true |
| $R_{\mathrm{b}}$ | $0.2140 \pm 0.0038$ | $0.2059 \pm 0.0018$ | 0.2069 |
| $\epsilon^{\mathrm{b}}$ | $0.1640 \pm 0.0028$ | $0.1609 \pm 0.0013$ | 0.1602 |
| Assume different efficiencies for both jets | | | |
| $l/\sigma > 3$ | DATA | MC | MC, true |
| $R_{\mathrm{b}}$ | $0.2149 \pm 0.0031$ | $0.2054 \pm 0.0017$ | 0.2069 |
| $\epsilon_1^{\mathrm{b}}$ | $0.3019 \pm 0.0039$ | $0.3022 \pm 0.0021$ | 0.3002 |
| $\epsilon_2^{\mathrm{b}}$ | $0.2162 \pm 0.0027$ | $0.2108 \pm 0.0013$ | 0.2095 |
| $a^{\mathrm{NN}} > 0.7$ | DATA | MC | MC, true |
| $R_{\mathrm{b}}$ | $0.2159 \pm 0.0038$ | $0.2058 \pm 0.0018$ | 0.2069 |
| $\epsilon_1^{\mathrm{b}}$ | $0.2037 \pm 0.0036$ | $0.2043 \pm 0.0017$ | 0.2033 |
| $\epsilon_2^{\mathrm{b}}$ | $0.1215 \pm 0.0022$ | $0.1177 \pm 0.0010$ | 0.1171 |

Table 2: *Results of the $R_{\mathrm{b}}$ analysis for the four-jet events. Shown are the rates for primary $\mathrm{b\overline{b}}$ production and the efficiencies to tag jets in $\mathrm{b\overline{b}}$ events, measured from the data and the simulated events. Also shown are the corresponding true values in the simulation. The errors are statistical errors only. Two models for the per-jet tagging efficiency are studied for two different cuts each.*

is to require $l/\sigma > 3$ for the decay length significance of the secondary vertex associated with the track. The second method is to require in addition to the $l/\sigma$ cut $a^{\mathrm{NN}} > 0.7$ for the neural network output. The same cut values on these variables have been used to select the $\mathrm{g} \to \mathrm{b\overline{b}}$ events. Table 2 shows the measured $R_{\mathrm{b}}$ and tagging efficiencies for $\mathrm{b\overline{b}}$ events when performing the double tag analysis on the data and the Monte Carlo samples. Also shown are the true value of $R_{\mathrm{b}}$ and the true tagging efficiencies in the Monte Carlo sample. No systematic uncertainties are shown. The efficiencies observed in the data are slightly higher than in the Monte Carlo simulation, independent of the analysis method. The measured parameter $R_{\mathrm{b}}$ is also higher in the data than in the simulation. The relative deviations observed are 3% or less for the efficiencies and 5% or less for $R_{\mathrm{b}}$.

The apparently larger value observed for $R_{\mathrm{b}}$ in the data does not necessarily correspond to a different rate of b quarks in the Monte Carlo simulation than in the data. It could also be explained by larger efficiencies to tag charm or light quarks than simulated. To cover possible differences in the flavour composition of the four jet sample in the data compared to the simulation, the primary production of $\mathrm{b\overline{b}}$ quark pairs $R_{\mathrm{b}}$ has been varied in the simulation by 5%. This leads to uncertainties $\Delta g_{\mathrm{b\overline{b}}} = 0.17 \times 10^{-3}$ and $\Delta g_{4\mathrm{b}} = 0.06 \times 10^{-3}$, shown in table 3. Uncertainties in the tagging efficiencies due to the modelling of the OPAL detector and heavy flavour physics are covered in section 4.4 and 4.5.

### 4.2 Dependence on the b quark mass

The influence of the b quark mass assumed for the Monte Carlo simulation has been studied by changing the b quark's current algebra mass in the JETSET program and investigating the properties of the b hadrons produced in the fragmentation process. Figure 8 shows the momenta of the two b hadrons in $\mathrm{g} \to \mathrm{b\overline{b}}$ events and their invariant mass for three different choices of this parameter in JETSET. If more than two such hadrons are present

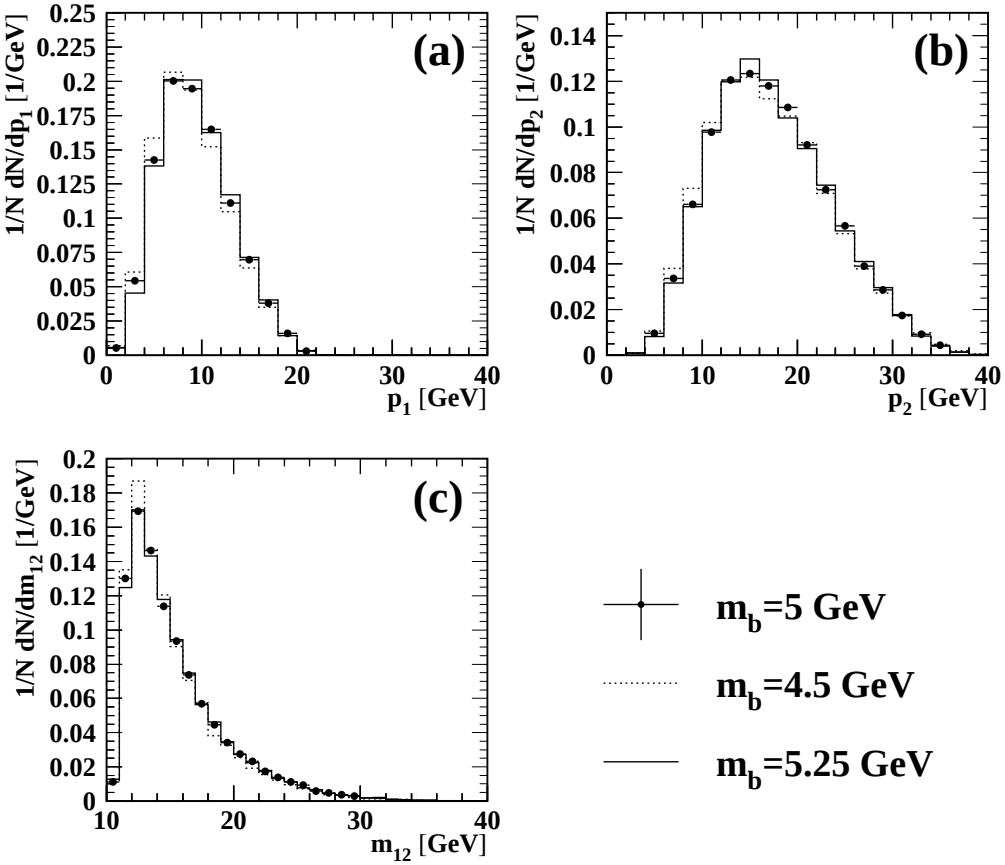


Figure 8: *The momentum of the two* b *hadrons from the* $g \to b\bar{b}$ *process,* $p_1$ *and* $p_2$*, shown in figure (a) and (b), respectively, and their invariant mass* $m_{12}$*, shown in figure (c), for three different choices of the* b *quark's current algebra mass in* JETSET*. The momenta are ordered such that* $p_1 < p_2$*. If more than two* b *hadrons are present in the event, only the pair with the lowest invariant mass is considered. The default mass in* JETSET 5 GeV *is shown as dots with error bars, the masses* 4.5 GeV *and* 5.25 GeV *as dotted and solid lines.*

(for $b\bar{b}b\bar{b}$ events) only the two b hadrons with the lowest momentum are considered. These variables were chosen, because the efficiency to identify b hadrons is very sensitive to their momentum. The efficiency to resolve the two b hadrons in different jets depends strongly on their invariant mass. It is clearly visible that a lower b quark mass in JETSET results in a softer spectrum for all three variables. The central value for the b quark mass in JETSET used throughout this analysis is 5 GeV. The shapes of the distributions shown have been used to re-weight the $g \to b\bar{b}$ Monte Carlo events corresponding to a b quark mass of 4.5 GeV and 5.25 GeV. This variation covers the uncertainty on the b quark pole mass [20] as well as the mass range considered for the effective b quark mass in QCD calculations of $g_{b\bar{b}}$ [1]. The variation of the b quark mass parameter leads to systematic uncertainties $\Delta g_{b\bar{b}} = 0.10 \times 10^{-3}$ and $\Delta g_{4b} = 0.06 \times 10^{-3}$ as shown in table 3.

### 4.3 Model dependence

Though the parton shower approach, as implemented in JETSET, describes the gluon splitting process quite well [1], it is desirable to look at other models and at exact calculations.

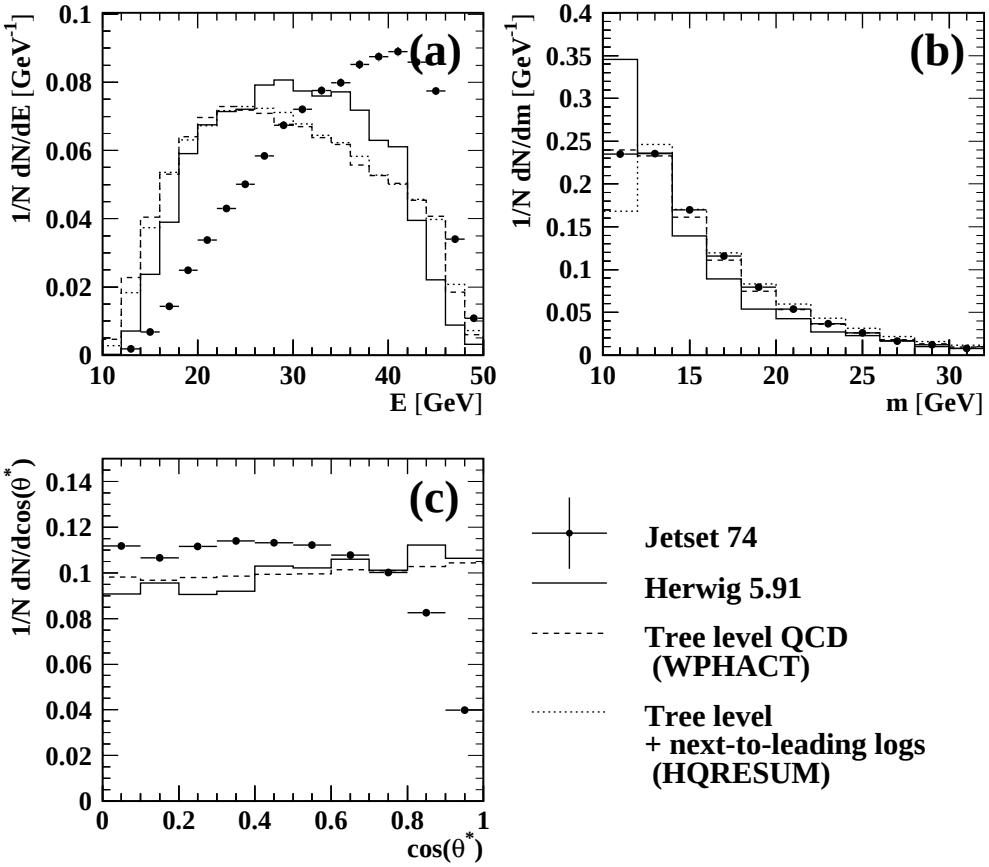


Figure 9: *(a) the energy E of the gluon that splits to* $b\bar{b}$*, (b) the gluon virtuality m, (c) the decay angle* $\cos(\theta^\star)$ *of the* $b\bar{b}$ *pair in the gluon rest-frame, for different models and calculations, described in the text. The next-to-leading order calculation is not available for the variable* $\cos(\theta^\star)$ *and it does not include* $b\bar{b}b\bar{b}$ *final states. The first bin of (b) is lower for the next-to-leading order prediction as described in the text.*

Version 5.91[2] of the HERWIG [21] Monte Carlo generator provides an alternative model for the parton shower. The program WPHACT [22] implements $e^+e^-$ annihilation to four fermions, where the masses of b quarks are taken into account fro the calculation of the matrix elements. It can be used to study $b\bar{b}b\bar{b}$ and $b\bar{b}q\bar{q}$ final states. Version 1.3 of WPHACT[3] [23] implements the possibility to switch off graphs where the b quarks couple to the $Z^0$ or $\gamma$, it therefore can be used to study the gluon splitting process in isolation on tree level. For the case of light primary quarks, calculations are available where next to leading order logarithmic terms have been taken into account [1, 24]. The program HQRESUM[4] [25] calculates three-jet like observables including next to leading order logarithmic corrections.

Figure 9 shows differential distributions of kinematic variables of the gluon that splits to $b\bar{b}$, calculated with JETSET, HERWIG, WPHACT[5] and HQRESUM. For $b\bar{b}b\bar{b}$ events generated

[2]This version includes an enhanced treatment of the gluon splitting process, as already mentioned in [6] and has been given to us by courtesy of the author.

[3]Provided to us by courtesy of the author.

[4]Provided to us by courtesy of the author.

[5]The following cuts are applied on the invariant masses of pairs of the four partons with the program WPHACT: $m_{qq} > 1.9\,\text{GeV}$, $m_{bq} > 5.87\,\text{GeV}$ and $m_{bb} > 10\,\text{GeV}$. Here q (b) stands for a light (b flavoured) quark or anti-quark.

with WPHACT the $b\bar{b}$ pair with the lowest invariant mass was chosen to calculate the "gluon". The predictions from WPHACT and HQRESUM are in good agreement for the gluon energy (figure 9a). The same is true for the gluon virtuality (figure 9b), except for the first bin. There the re-summed contributions in HQRESUM are not calculated for gluon virtualities $m < 2.3 \times m_b$, because non-perturbative effects are large [24]. JETSET predicts a harder energy spectrum for the gluon than the QCD calculations, while the HERWIG prediction is closer to these calculations but still prefers higher energies. This is different for the gluon virtuality distribution, here JETSET predicts a harder spectrum than HERWIG, in agreement with the QCD calculations. For the decay angle in the gluon rest-frame (figure 9c) HERWIG and WPHACT predict a nearly flat distribution, while JETSET predicts a lower rate of events with the $b\bar{b}$ axis parallel to the gluon axis. No HQRESUM calculation is available for this variable. The distributions of the kinematic variables shown in figure 9 have been varied from the JETSET prediction to reflect the distributions predicted by HERWIG and WPHACT. This results in uncertainties $\Delta g_{b\bar{b}} = 0.36 \times 10^{-3}$ and $\Delta g_{4b} = 0.12 \times 10^{-3}$, which are shown in table 3.

### 4.4 Experimental sources of systematic uncertainties

The following experimental sources of systematic uncertainties have been investigated. The resulting uncertainties are summarised in table 3.

**The statistical error** on the selection efficiencies in the 25 bins used for the likelihood analysis, determined with Monte Carlo simulations, leads to uncertainties in $g_{b\bar{b}}$ and $g_{4b}$.

**The four-jet selection** is defined using a cut $y_{34} > y_{34}^{\min}$. Figure 10a shows the number of events in the data divided by the predicted number of events as a function of this cut. The disagreement in the rate of four-jet events, as discussed in section 2.4, is clearly visible. The fit results for $g_{b\bar{b}}$ and $g_{4b}$ as a function of this cut are studied in figure 10b and 10c. The fit results are stable under the variation of $y_{34}^{\min}$ within the independent statistical error. This shows that the treatment of the normalisation to the four-jet rate in the likelihood fit is correct, so no systematic error on $g_{b\bar{b}}$ and $g_{4b}$ is assigned.

**The normalisation** to the number of four jet events revealed differences in the population of the event classes "2+2" and "3+1" when comparing the data with the Monte Carlo prediction, as discussed in section 3.1. Therefore the likelihood fit was repeated, using the event-numbers and selection efficiencies of the classes "2+2" and "3+1", rather than the number of four-jet events and the corresponding selection efficiencies.

**The modelling of the OPAL detector** is important in this analysis because the analysis depends on an accurate modelling of the vertex reconstruction. The b tagging efficiencies are modelled correctly only within about 3%, as shown in section 4.1. They are mainly sensitive to the parameters modelling the production and decay of b hadrons. This is studied in section 4.5. The light quark tagging efficiencies in the Monte Carlo simulation are mainly sensitive to details in the modelling of the tracking system. Studies have been done by smearing the reconstructed track parameters in the Monte Carlo simulation with respect to the true track parameters in the simulation. The double tag analysis from section 4.1 was then repeated, to cross-check the agreement between data and the smeared simulation. Instead of only calculating $R_b$ and the b tagging efficiency, additional tests have been performed by taking $R_b$ in the four-jet sample from the simulation and calculating the charm or light quark tagging

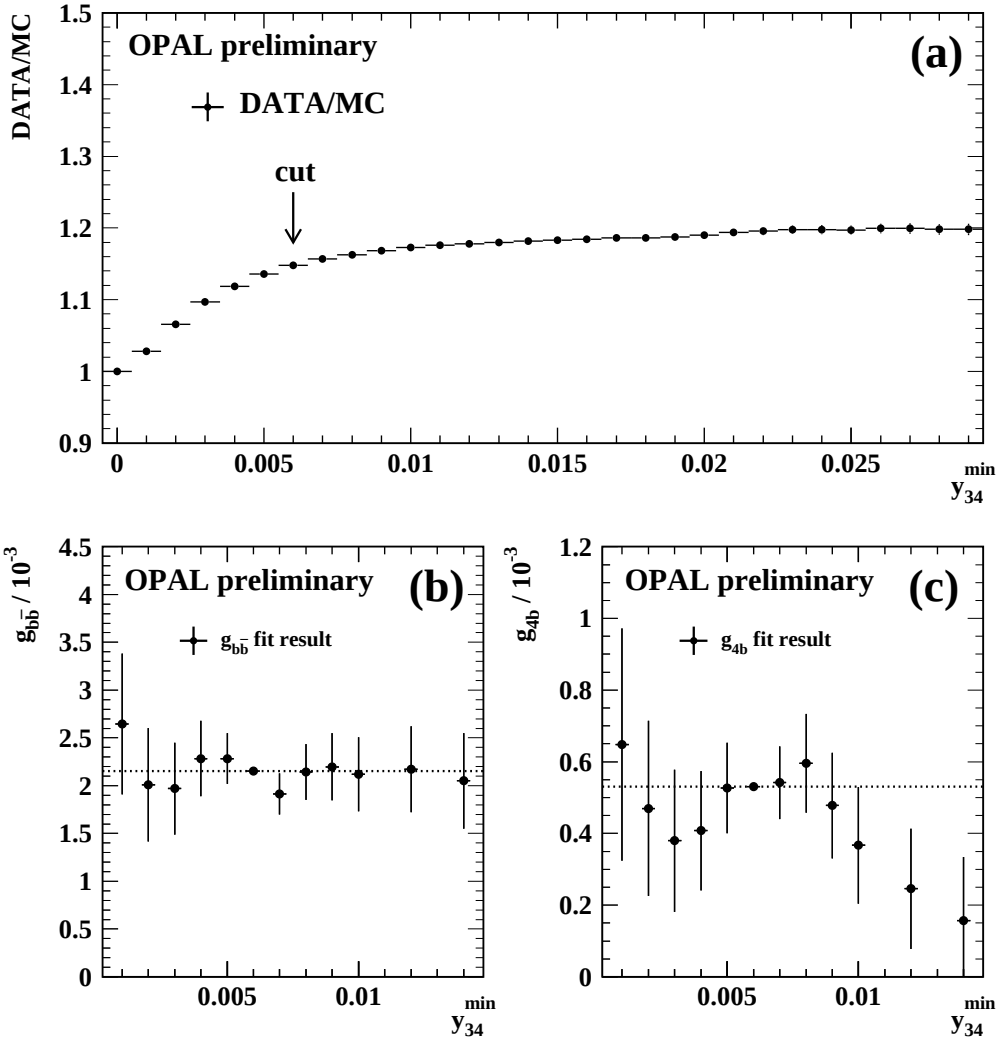


Figure 10: *Dependence of the four-jet rate and the fit results on $y_{34}^{\min}$, the lower cut in the jet resolution parameter $y_{34}$. Figure (a) shows the ratio of the number of events in the data by the number of events predicted from the Monte Carlo simulation, the figures (b) and (c) show the fit result for $g_{\mathrm{b\bar{b}}}$ and $g_{4\mathrm{b}}$. The error bars in (b) and (c) correspond to the statistical errors independent from the central value $y_{34}^{\min} = 0.006$.*

efficiencies from the data. A smearing of 3% for the cut $l/\sigma > 3$ and of 8% for the cut $a^{\mathrm{NN}} > 0.7$ was found to describe the charm and light quark tagging efficiencies correctly. Finally the gluon splitting analysis was repeated using the modified Monte Carlo sets.

**The $k_\perp$ algorithm** is used in this analysis not only to define the jets, but also to calculate the event topology. Therefore it is important to test the analysis, using a different algorithm. The JADE E0 [26] jet clustering scheme has been used as an alternative method, with a cut $y_{34} > 0.015$ to define four-jet events. This resulted in 277 selected events. Only 88 of these events were already selected within the 310 events mentioned in section 3.3. The result of the likelihood fit using the JADE E0 algorithm is $g_{\mathrm{b\bar{b}}}^{\mathrm{JADE}} = (2.76 \pm 0.48) \times 10^{-3}$ and $g_{4\mathrm{b}}^{\mathrm{JADE}} = (0.38 \pm 0.19) \times 10^{-3}$ (statistical errors only). These results are compatible with the results obtained with the $k_\perp$ algorithm

within the statistical errors, considering the small fraction of events common to both selections. No systematic error is assigned from this test.

| source of systematic error | $g_{b\bar{b}}$ uncertainty | $g_{4b}$ uncertainty |
|---|---|---|
| b quark mass | $0.10 \times 10^{-3}$ | $0.06 \times 10^{-3}$ |
| Model dependence | $0.36 \times 10^{-3}$ | $0.12 \times 10^{-3}$ |
| $g \to b\bar{b}$ Monte Carlo statistics | $0.07 \times 10^{-3}$ | $0.02 \times 10^{-3}$ |
| $b\bar{b}b\bar{b}$ Monte Carlo statistics | $0.03 \times 10^{-3}$ | $0.04 \times 10^{-3}$ |
| $g \to c\bar{c}$ Monte Carlo statistics | $0.11 \times 10^{-3}$ | $0.04 \times 10^{-3}$ |
| Other background Monte Carlo statistics | $0.15 \times 10^{-3}$ | $0.06 \times 10^{-3}$ |
| DATA/MC normalisation | $0.18 \times 10^{-3}$ | $0.05 \times 10^{-3}$ |
| Detector simulation | $0.54 \times 10^{-3}$ | $0.12 \times 10^{-3}$ |
| $g_{c\bar{c}} = (2.38 \pm 0.48) \times 10^{-2}$ | $0.07 \times 10^{-3}$ | $0.007 \times 10^{-3}$ |
| Charm hadrons lifetime | $0.05 \times 10^{-3}$ | $0.02 \times 10^{-3}$ |
| Charm fragmentation | $0.06 \times 10^{-3}$ | $0.007 \times 10^{-3}$ |
| Charm production rates | $0.02 \times 10^{-3}$ | $0.003 \times 10^{-3}$ |
| Charm decay multiplicities | $0.08 \times 10^{-3}$ | $0.03 \times 10^{-3}$ |
| $R_b$ in the four-jet sample | $0.17 \times 10^{-3}$ | $0.06 \times 10^{-3}$ |
| Bottom hadron lifetime | $0.09 \times 10^{-3}$ | $0.05 \times 10^{-3}$ |
| Bottom fragmentation | $0.22 \times 10^{-3}$ | $0.06 \times 10^{-3}$ |
| Bottom production rates | $0.06 \times 10^{-3}$ | $0.03 \times 10^{-3}$ |
| Bottom decay multiplicities | $0.09 \times 10^{-3}$ | $0.04 \times 10^{-3}$ |
| Total systematic error | $\mathbf{0.80 \times 10^{-3}}$ | $\mathbf{0.23 \times 10^{-3}}$ |

Table 3: *Summary of the systematic errors*

### 4.5 Uncertainties from heavy flavour physics

The following sources of systematic uncertainties from heavy flavour physics have been investigated. The results are shown in table 3.

**Secondary and primary $c\bar{c}$ and $b\bar{b}$ production rates:** the rate of secondary produced $c\bar{c}$ quark pairs, $g_{c\bar{c}}$, has been measured to be $g_{c\bar{c}} = (2.38 \pm 0.48) \times 10^{-2}$ [16]. It has been changed within these experimental errors. The explicit dependence of the results on $g_{c\bar{c}}$ is given by

$$\frac{\partial g_{b\bar{b}}}{\partial g_{c\bar{c}}} = -0.0147, \quad \frac{\partial g_{4b}}{\partial g_{c\bar{c}}} = -0.00135.$$

Varying the rate of primary $c\bar{c}$ production only has a negligible effect on the results. The the rate of primary $b\bar{b}$ production was measured in section 4.1 for the four jet sample using a double-tag technique. The differences of the predicted to the measured rate $R_b^{4-\mathrm{jet}}$ have been considered by adjusting the rate of primary $b\bar{b}$ production in the simulation in the range $\pm 5\%$. The full difference on the result has been assigned as a systematic error.

**The lifetimes** of charm and bottom hadrons are varied around their central value according to the numbers given by the Particle Data Group [20].

**The fragmentation functions** for charm and bottom quarks have been varied to reflect the uncertainties in the knowledge of the average scaled energies for D and B mesons

(taken from [27]). This has been done by varying the parameter $\epsilon$ in the parametrisation of the fragmentation function suggested by Peterson [28]. In addition the sensitivity to the shape of the fragmentation function has been checked, using the models suggested by Collins and Spiller [29] and Kartvelishvili [30]. The uncertainties from the knowledge of the mean scaled energies and the shape of the distributions have been added in quadrature.

**The production rates** of charmed and bottom hadrons are varied within the range given in [27] and [20].

**The charged decay multiplicities** of the D mesons have been varied within their errors [31]. The mean charged decay multiplicity of weakly decaying b hadrons is varied within $n_B = 4.995 \pm 0.062$ [27]. Variations of the neutral decay multiplicities have not been studied.

Finally, all systematic errors were added in quadrature, which leads to the results

$$\begin{aligned} g_{\mathrm{b\overline{b}}} &= (2.15 \pm 0.43(\mathrm{stat.}) \pm 0.80(\mathrm{syst})) \times 10^{-3}, \\ g_{4\mathrm{b}} &= (0.53 \pm 0.20(\mathrm{stat.}) \pm 0.23(\mathrm{syst})) \times 10^{-3}. \end{aligned}$$

The statistical errors have a correlation 0.066. The systematic uncertainties in most cases influence the selection efficiencies for both the $\mathrm{g} \to \mathrm{b\overline{b}}$ and the $\mathrm{b\overline{b}b\overline{b}}$ signal in the same direction, which results in correlated shifts of $g_{\mathrm{b\overline{b}}}$ and $g_{4\mathrm{b}}$ to higher or lower values.

# 5 Summary

A measurement of the inclusive rate of gluons splitting to $\mathrm{b\overline{b}}$ per hadronic $\mathrm{Z}^0$ decay has been performed using data taken by OPAL. The result is

$$g_{\mathrm{b\overline{b}}} = (2.15 \pm 0.43(\mathrm{stat.}) \pm 0.80(\mathrm{syst})) \times 10^{-3}.$$

Simultaneously the rate of events with four bottom quarks has been measured, with the result

$$g_{4\mathrm{b}} = (0.53 \pm 0.20(\mathrm{stat.}) \pm 0.23(\mathrm{syst})) \times 10^{-3}.$$

The result for $g_{\mathrm{b\overline{b}}}$ is compatible with previous measurements reported by ALEPH $g_{\mathrm{b\overline{b}}} = (2.77 \pm 0.42(\mathrm{stat}) \pm 0.57(\mathrm{syst})) \times 10^{-3}$ [6] and DELPHI $g_{\mathrm{b\overline{b}}} = (2.1 \pm 1.1(\mathrm{stat}) \pm 0.9(\mathrm{syst})) \times 10^{-3}$ [5]. It is also consistent with theoretical predictions $g_{\mathrm{b\overline{b}}}^{\mathrm{theor}} = (1.8 - 2.9) \times 10^{-3}$ [1, 4]. The result for $g_{4\mathrm{b}}$ is compatible with the naive expectation $g_{4\mathrm{b}} \approx R_{\mathrm{b}} \times g_{\mathrm{b\overline{b}}}$.

# References


[1] M. H. Seymour, Nucl. Phys. **B436** (1995) 163-183.

[2] B. A. Kniehl and J. H. Kühn, Nucl. Phys. **B329** (1990) 547-573.

[3] T. Sjöstrand, Comp. Phys. Comm. **39** (1986) 347;
T. Sjöstrand, Comp. Phys. Comm. **82** (1994) 74.

[4] S. Frixione *et al.*, Heavy quark production, CERN-TH-97-16, Feb. 1997.

[5] DELPHI Collaboration, P. Abreu *et al.*, Phys. Lett. **B405** (1997) 194.

[6] ALEPH Collaboration, CERN-EP/98–103.

[7] M. Bengtsson and P. Zerwas, Phys. Lett. **B208** (1988) 306.

[8] OPAL Collaboration, G. Alexander *et al.*, Z Phys. **C52** (1991) 275.

[9] P. P. Allport *et al.*, Nucl. Instr. and Meth. **A324** (1993)34.

[10] P. P. Allport *et al.*, Nucl. Instr. and Meth. **A346** (1994)476.

[11] S. Anderson *et al.*, Nucl. Instr. and Meth. **A403** (1998) 325.

[12] OPAL Collaboration, G. Alexander *et al.*, Z. Phys. **C52** (1991) 175.

[13] OPAL Collaboration, K. Ackerstaff *et al.*, Euro. Phys. J. **C2** (1998) 213-236.

[14] J. Allison *et al.*, Nucl. Instr. and Meth. **A317** (1992) 47.

[15] The LEP Electroweak Working group, CERN-EP/99-15.

[16] The OPAL Collaboration, R. Akers *et al.*, Z. Phys. **C67** (1995) 27-44;
The OPAL Collaboration, R. Akers *et al.*, Phys. Lett. **B353** (1995) 595-605.

[17] S. Catani *et al.*, Phys. Lett. **B 269** (1991) 432;
N. Brown and W. J. Stirling, Z. Phys. **C 53** (1992) 629.

[18] OPAL Collaboration, K. Ackerstaff *et al.*, Z.Phys. **C74** (1997) 1.

[19] The OPAL Collaboration, G. Abbiendi *et al.*, CERN-EP/98-137 (accepted by Euro. Phys. J. C).

[20] Particle Data Group, C. Caso *et al.*, Euro. Phys. J. **C3** (1008) 1.

[21] G. Marchesini, B. R. Webber, G. Abbiendi, I. G. Knowles, M. H. Seymour, and L. Stanco, Comp. Phys. Comm. **67** (1992) 465;
M. H. Seymour, private communication.

[22] E. Accomando and A. Ballestrero, Comp. Phys. Comm. **99** (1997) 270.

[23] A. Ballestrero, private communication.

[24] D. J. Miller and M. H. Seymour, Phys. Lett. **B435** (1998) 213.

[25] D. J. Miller, private communication.

[26] JADE collab., W. Bartel *et al.*, Z. Phys. **C33** (1986) 23;
JADE collab., S. Bethke *et al.*, Phys. Lett. **B213** (1988) 235.

[27] The LEP collaborations, ALEPH,DELPHI, L3 and OPAL, Nucl. Instr. Meth. **A378** (1996) 101;
Updated averages are described in 'Presentation of LEP Electroweak Heavy Flavour Results for Summer 1998 Conferences', LEPHF 98-01
(see `http://www.cern.ch/LEPEWWG/heavy/`).

[28] C. Peterson, D. Schlatter, I. Schmitt and P. Zerwas, Phys. Rev. **D27** (1983) 105.

[29] P. Collins and T. Spiller, J. Phys. **G11** (1985 1289.

[30] V. G. Kartvelishvili, A. K. Likhoded and V. A. Petrov, Phys. Lett. **B78** (1978) 615.

[31] MARK III collaboration, D. Coffman *et al.*, Phys. Lett. **B263** (1991) 135.